Renewable Energy 148 (2020) 1137–1149

Contents lists available at ScienceDirect

Renewable Energy

journal homepage: www.elsevier.com/locate/renene

Significant decrease of photovoltaic power production by aerosols. The case of Santiago de Chile

Mirko Del Hoyo [a, *], Roberto Rondanelli [a, b], Rodrigo Escobar [c]

[a] Departamento de Geofísica, Universidad de Chile, Av. Blanco Encalada, 2002, Santiago, Chile
[b] Center for Climate and Resilience Research, Av. Blanco Encalada, 2002, Santiago, Chile
[c] Centro de Energía UC, Escuela de Ingeniería, Pontificia Universidad Católica de Chile, Av. Vicuña Mackenna, 4860, Santiago, Chile

ARTICLE INFO

Article history:
Received 8 March 2019
Received in revised form
14 September 2019
Accepted 2 October 2019
Available online 9 October 2019

Keywords:
Solar irradiance
Aerosols
Photovoltaics
AERONET
Air pollution
Santiago
Chile

ABSTRACT

Santiago de Chile frequently suffers from atmospheric pollution that contributes to the decrease of solar irradiance on the surface, leading to losses in the energy output of photovoltaic systems. In this study, a simple model is used to estimate the effect of aerosols on the solar irradiance over the city throughout the year, using as input AERONET sunphotometer data and other in-situ measurements. The results show reductions of 3.5% and 14.1% for global horizontal and direct normal irradiance respectively and an increase of 35.4% for diffuse horizontal irradiance between the actual condition in Santiago and a hypothetical atmosphere free of aerosols. These effects translate approximately to an annual difference in the energy output of −7.2% and −8.7% for monocrystalline and amorphous silicon PV technologies respectively, and an annual difference of −16.4% for a CPV technology, showing that aerosols can have a significant effect on the photovoltaic energy production.

1. Introduction

According to its 2050 energy policy, Chile has set a goal of having 70% of energy production by renewable sources by year 2050 [1]. This goal and the new Net Metering law has raised the interest of investors in different renewable energy systems such as solar, wind, biomass and ocean wave.

In terms of solar energy, Chile hosts the highest values of surface solar irradiance of the planet in parts of the Atacama Desert [2], with a maximum of 7.44 kWh/m^2/day. Important cities within the country also have high values of solar radiation throughout the year, with an annual average daily total for Santiago of 5.12 kWh/m^2/day [3,4]. Studies also show great potential for residential and commercial photovoltaic (PV) systems along the country [5]. Moreover, several major cities in Chile could supply 22% of the current electricity demand using PV technologies [6].

Given the good potential of PV systems in Chile, the net photovoltaic capacity has increased from 2.9 MW in December 2012 to 1802 MW in November 2017 [7]. Several factors may explain this increase, namely: The high solar irradiance over large parts of the country; the lower prices for photovoltaic modules; the low cost projections for PV systems [8]; the high energy demand from the mining industry; and the high price of electricity [9]. However, the PV market in Chile still has multiple technical and economic barriers, such as limited transmission capacity, volatile energy prices, an immature solar market and the effect of the environment on the energy production [10].

Quantifying the interaction of the environment with the surface solar irradiance and PV systems is needed to ensure technical feasibility and economic return. One variable of importance are aerosols, as they play an important role in the solar radiation budget. Different studies have shown a decrease of the shortwave irradiance and the photosynthetical active radiation (PAR) with the increase of the aerosol optical depth (AOD) (e.g Northern China [11], Australia [12] and Spain [13]). The decrease of the shortwave irradiance due to aerosols could also produce a decrease of the PV power output. In Eastern China, there are cases registered in which the reduction on the PV power output due to air pollution was around 35% [14].

Since the 1990s, several organizations have made efforts to improve the monitoring and abatement of air quality in Santiago, with emphasis on fine particulate matter at the surface due to

* Corresponding author.
E-mail address: mirko.delhoyo@ug.uchile.cl (M. Del Hoyo).

https://doi.org/10.1016/j.renene.2019.10.005
0960-1481/

health concerns. Nevertheless, high concentrations of aerosols are still a problem due to the prevalence of thermal inversion conditions [15], low boundary layer heights [16] and the multiple emission sources of pollutants in the city [17–19].

Santiago provides particularly a good site to study the effect of aerosols on the solar irradiance given its high frequency of clear sky days (approximately 200 days per year) and a long series of aerosol measurement. Nonetheless, few studies related to the effect of aerosols on the solar irradiance have been conducted in Santiago, with studies to date only showing the effect of aerosols on UV radiation [20]. Others studies conducted in Santiago by Molina [21][and Molina et al. [22] found a significant bias of around 30% between a semi-empirical solar irradiance model and the observed GHI, which they hypothesized to the scattering/absorption due to aerosols.

Besides their effect on the solar irradiance, aerosols can impact the power output of PV generation systems by the deposition of particles on the modules [23,24]. For instance, Urrejola et al. [25] studied the effect of soiling and degradation for thin film (TF), polycrystalline (p-Si) and monocrystalline (m-Si) silicon photovoltaic arrays in Santiago, obtaining a mean annual average decay of the performance ratio (PR) of 7.9%, 6.8% and 7.1%, with a maximum decay of 16.8%, 12.3% and 12.9% in autumn of 2015 for each technology respectively. These results show a larger PR reduction when compared to similar studies in other regions of the world [26–29], which may have been associated with the high levels of air pollution [25]. Besides these studies there is no research related with the effect of the atmospheric column of aerosols on the power output of photovoltaic systems in Chile.

In this paper, we estimate the effects of aerosols for different surface solar irradiance components under clear sky using observations and SMARTS2, a model for solar irradiance based on several surface measurements, such as AOD, water vapor and ozone. With the solar irradiance model, it is possible to calculate the power output of different photovoltaic technologies with the current atmospheric conditions and also estimate the power output in a case with no-AOD in Santiago.

The paper is organized as follows. Section 2 describes the site and the data used. The methodology is detailed in Section 3. Results from the solar irradiance model, PV model and the CPV model are found in Section 4. Section 5 contains the main conclusions of this work.

2. Site description and data

Santiago, Chile (−33.45°N, −70.66°W) is located in a basin surrounded by the Andes to the east and a coastal mountain range to the west, with heights of 1000 m a.s.l and 4000 m a.s.l respectively. Mean climate in Santiago is semi-arid, with an average precipitation of 320 mm concentrated during wintertime and a long dry season that extends from spring to fall. Mean temperatures range between 5°C and 27°C (See Fig. 1). The effect of the Southeastern Pacific subtropical anticyclone, located in front of the Chilean coast at around 30°, contributes to the large number of clear days throughout the year due to the prevalence of a subsidence inversion in the lower troposphere. Together with the quasi-permanent influence of the Pacific high, the passage of coastal lows (a subsynoptic feature traveling southward with a nearly weekly frequency) intensifies the large scale subsidence [15], producing favorable conditions for the accumulation of air pollutants, especially during wintertime, where boundary layer growth and vertical dispersion of pollutants is inhibited by the lower values of surface radiation [16,18,30].

To study the effect of aerosols on the solar irradiance, different datasets were obtained between 2014 and 2016 in two different locations: one at the Beauchef Campus of Universidad de Chile (−33.4572°N, −70.6616°W) and the other at the San Joaquin Campus of Pontificia Universidad Católica de Chile (−33.4976°N, −70.6066°W). Both sites have nearly the same altitude and are separated by less than 7 km.

The global horizontal irradiance (GHI) and diffuse horizontal irradiance (DHI) were measured with a CMP21 Kipp and Zonen pyranometer. The diffuse component was measured using a full ball shadowing. The direct normal irradiance (DNI) was measured with a CHP1 Kipp and Zonen pyrheliometer. The accuracy of all the instruments is ±2%, and all are properly calibrated with traceability to the world radiation reference (WRR) at Davos. All the instruments were installed in a SOLYS2 Kipp and Zonen two-axis sun tracker. The pointing accuracy of the sun tracker is less than 0.1°. Each component was measured every second and averaged every minute.

The quality control for the solar irradiance dataset was proposed by Rojas et al. [31] and consists of 17 quality tests. To start the quality control, the first criterion filtered the data with solar elevations lower than 10°. Then, criterion 2 to 14 from Rojas et al. [31] were applied based on the hourly mean of each component, where each data was flagged as valid or invalid for each test. After that, daily means for the GHI, DNI and DHI were calculated for criterion 15 and 16, filtering all the hourly data in each day that did not pass the quality control. Finally, an envelope using the clearness index and the diffuse ratio was created, using the hourly data filtered. All the data flagged as erroneous was deleted, which in this study correspond to 64% of the entire dataset. It is important to note that we used the same quality-controlled dataset obtained by Rojas et al. for Santiago (same variables and period).

Air temperature and relative humidity were measured every 1 min using a Campbell CS215 installed at two meters. The accuracy of the instrument is ±0.4 °C for the air temperature and ±2% in a range of 10–90% and ±4% in a range of 0–100% for the relative humidity.

Wind velocity was measured with a Young 85,000, an ultrasonic anemometer installed at two meters over the PV plant. The instrument has an accuracy of ±2% for speeds between 0 and 30 m/s, and ±3% for the range of 30 – 70 m/s. The wind data was acquired at a frequency of 1 min.

Solar irradiance, air temperature, relative humidity, and wind velocity data was stored in a Campbell Scientific CR1000 at the Campus San Joaquín. The datalogger uncertainty lies by ±0.06% of reading plus offset.

Aerosol data, such as AOD, Angstrom coefficient, single scattering albedo (SSA), the asymmetry factor and water vapor data were obtained with an automatic sun photometer CIMEL CE-318-4 included in the AERONET (Aerosol Robotic Network), located at Beauchef Campus. Measurements are available from late 2013 to date of AOD at 340, 380, 440, 500, 675, 870, 1020 and 1640 nm, water vapor (w) and Angstrom coefficient every 15 min. The data is cloud screened and quality assured (Level 2.0). The accuracy of the instrument is between 0.01 and 0.02 [32]. Hourly means of AOD, water vapor, Angstrom coefficient and the monthly mean single scattering albedo (SSA) in Santiago throughout the year are shown in Fig. 2.

Regarding the PV power output measurements, photovoltaic modules were installed at Pontificia Universidad Católica de Chile. The power output data was obtained every 15 min from arrays used previously by Urrejola et al. [25], consisting of 2 different types of technologies, monocrystalline silicon (m-Si) and thin film amorphous silicon (a-Si). The arrays are tilted 32° toward the equator, with an azimuth of 350° (clockwise from due north).

All technologies were cleaned monthly by brushing with water and the raining events were recorded to take into account the effect

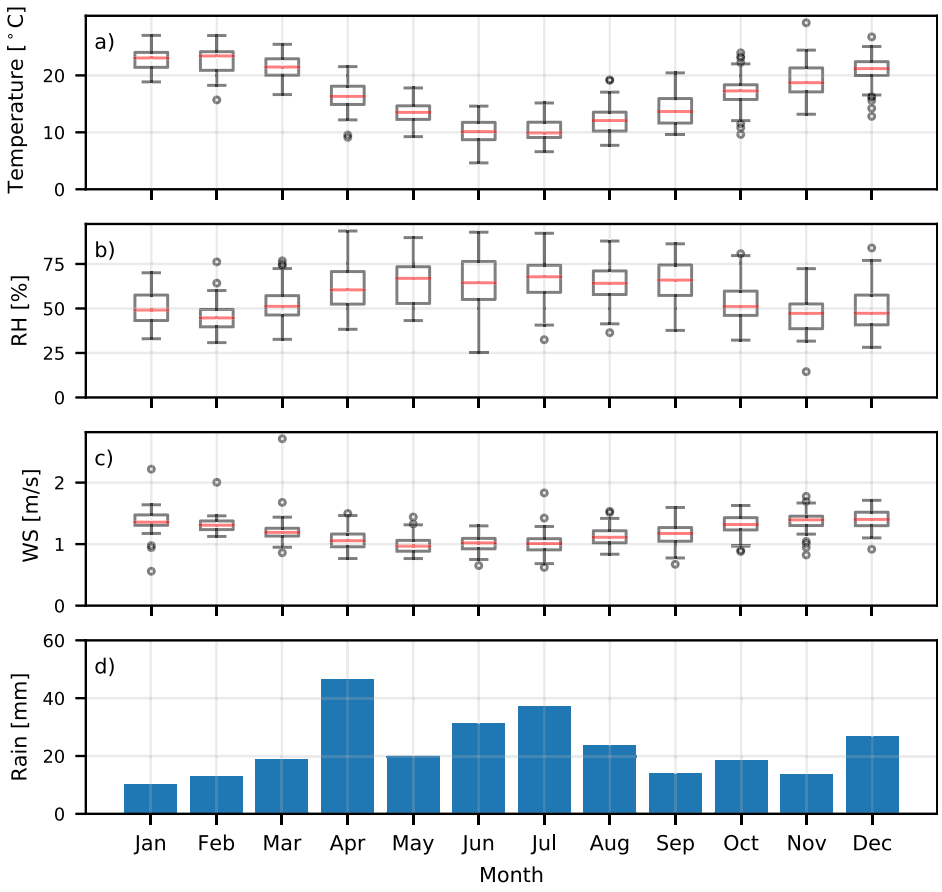

Fig. 1. Monthly boxplot obtained with daily mean values for a) 2 m Temperature, b) 2 m relative humidity (RH), and c) 2 m wind speed (WS). In d) Mean monthly precipitation. The data was obtained between 2014 and 2016.

of soiling. Moreover, the degradation and the temperature coefficient for the power (δ) of the different PV technologies were considered, using the values obtained by Urrejola et al. [25]. Table 1 shows the specifications of the different modules used in this study and Fig. 3 shows the PV plant located in the campus San Joaquín.

3. Methodology

3.1. Clear sky detection

Aerosols measurements are only taken in clear sky condition. However, some clouds could have been detected in San Joaquín but not in Beauchef station due to the distance between both meteorological stations. To avoid that, the clear sky detection algorithm proposed by Reno and Hansen [33] was used to filter cloudy conditions in San Joaquín. The main advantage of this method over others is the possibility to customize the model, allowing the detection of cloudy periods without misclassify them with extreme episodes of air pollution.

The model consist in five criteria to classify a period as clear or cloudy. The first one considers the mean value of GHI, classifying the day as cloudy if the value is significantly lower than the mean value. For the second criterion, the maximum value of GHI is analyzed to detect periods where the global irradiance increases due to the brightness produced by clouds, comparing it with a clear sky model. The third one consider the variability along a time period, comparing it with the variability of a clear sky model. The fourth criterion analyze the maximum difference between changes in GHI and the irradiance obtained with a clear sky model. Finally, the standard deviation of the temporal change of GHI is calculated, classifying the periods as cloudy if the standard deviation is over 8 W/m^2.

The model is currently available as a Python package [34], with multiple options of broadband clear sky models to make the comparisons required in each test. In this study, we selected the model proposed by Ineichen [35] and a time window to execute the test of five minutes. Fig. 4 shows the detection of clear periods during three days in January 2014 using the model proposed.

3.2. Horizontal distribution of AOD

Since the main sites are separated by 7 km, we have to account for the difference in aerosol load between both places throughout the day. For this, we use the Multiangle Implementation of Atmospheric Correction (MAIAC) AOD product generated by NASA, which use the satellites measurements from MODIS AQUA and TERRA missions. The product includes AOD at 470 nm, 550 nm and water vapor with spatial resolution of 1 km.

A validation of MAIAC in Santiago using AERONET data with the methodology presented in Martins et al. [36] is shown in Fig. 5. This validation only account for the data from the AQUA mission between 2014 and 2016, a spatial average of 3 km around the AERONET station and a temporal average of 1 h around the data obtained between the 11:00 and 14:00 GMT-4, which in total correspond to

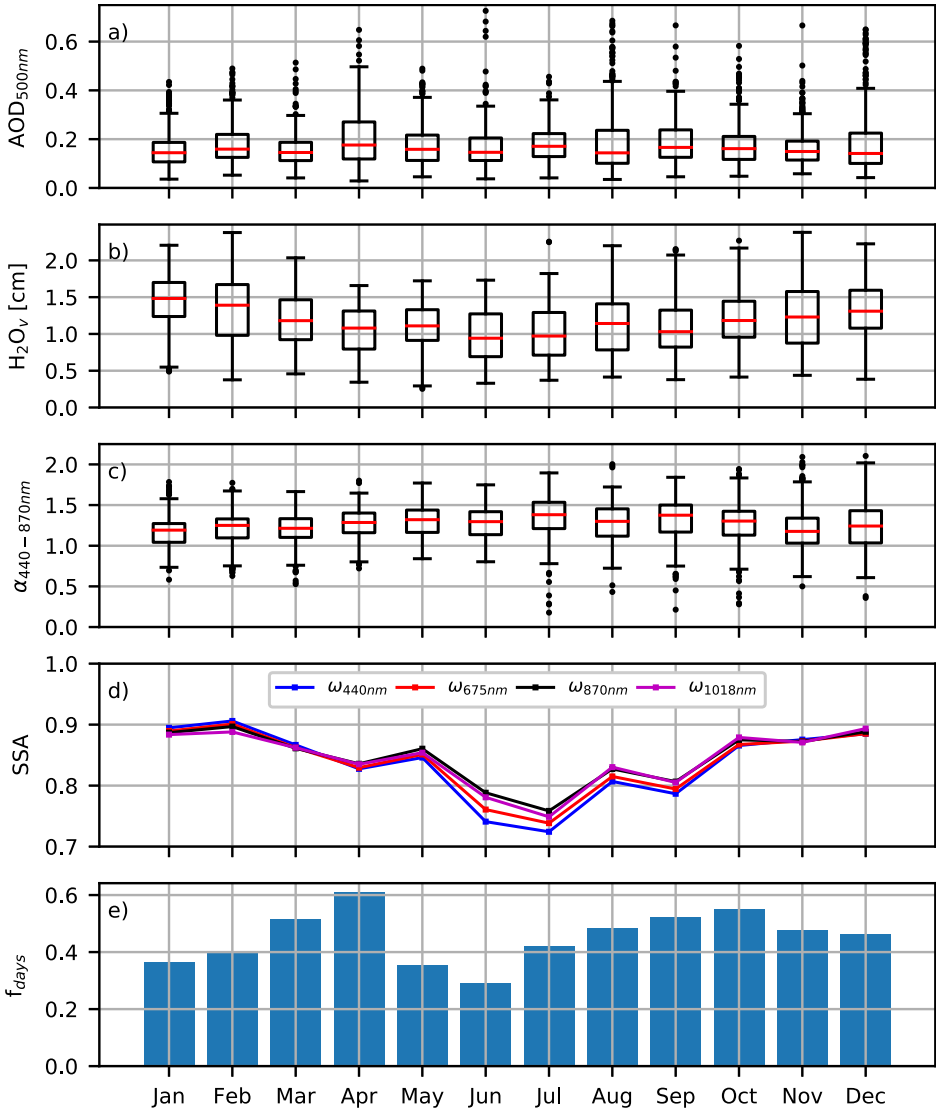

Fig. 2. Monthly boxplot obtained with hourly mean values for a) AOD 500 nm, b) water vapor, c) 440–870 nm Å coefficient. d) Monthly mean SSA (single scattering albedo) obtained by AERONET. e) Frequency of days per month with measurements. The data was obtained between 2014 and 2016.

Table 1
Specifications of the 2 PV technologies used in this study. Obtained from Urrejola et al. [25].

Name	Technology	N°	δ [%/°C]	P_{stc} [W_p]
m-Si	Cz-Si	6	−0.44	1590
a-Si	a-Si/μc-Si	12	−0.33	1380

156 days. Fig. 5.a shows that both places (San Joaquín and Beauchef) have a similar annual mean of AOD within this time range, with an annual mean between 0.12 and 0.14. The validation between MAIAC and AERONET, shown in Fig. 5b, is in agreement with the results presented by Martins et al. [36] for other urban cities over South America, with a relatively good coefficient of determination of 0.54. The dispersion shown in this figure is likely due to the problems that satellite aerosols retrievals have with urban covers [5,18]. Scatter plot in Fig. 5.c shows the AOD between San Joaquín and Beauchef using MAIAC, where a small difference less than 10% is found between both places. This allows us to compare surface solar irradiance and aerosol properties between both places.

Fig. 3. PV plant used in this study, located at San Joaquin campus of Pontificia Universidad Católica de Chile, Santiago, Chile.

3.3. Solar irradiance model

The SMARTS2 model [37] was used to obtain the clear sky solar irradiance in Santiago due to its versatility and availability of the

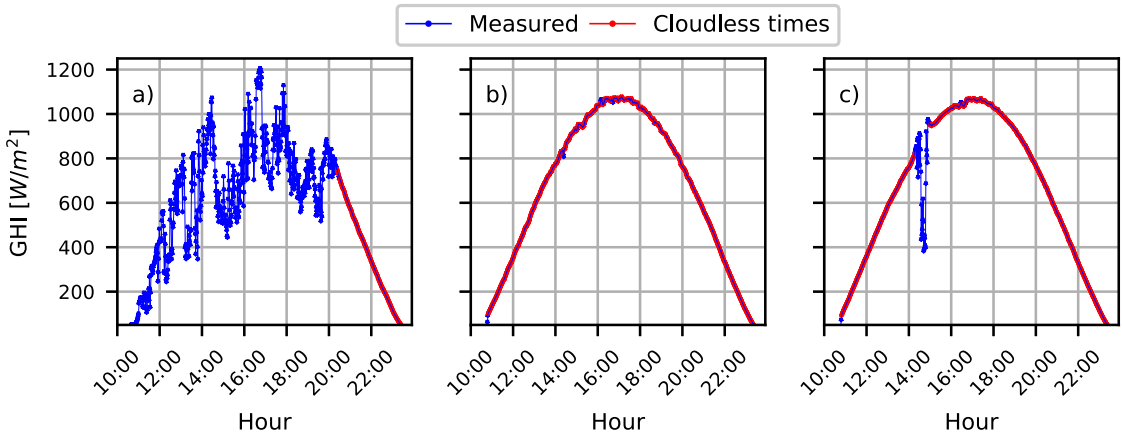

Fig. 4. Detection of cloud sky periods using the model proposed by Reno and Hansen [33] on a) January 23rd, b) January 24th and January 25th of 2014.

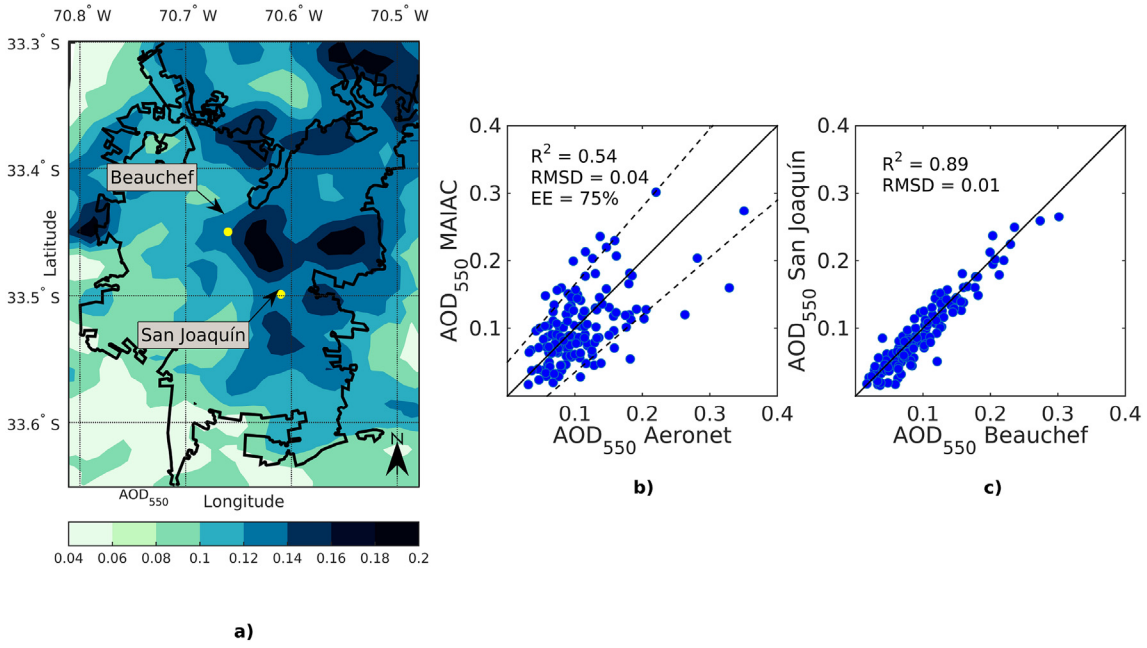

Fig. 5. a) Annual mean AOD obtained with MAIAC in Santiago using the AQUA product. b) difference between AERONET and the MAIAC product, the solid line represent a ratio 1:1 and the dashed ones represents the expected error (EE) of the model, defined as ± (0.05 + 0.15·AOD). c) the difference between Beauchef and San Joaquín using the MAIAC product. The solid line represents a ratio 1:1.

data required as input. The model calculates the clear sky spectrum based on parametrizations for the transmittance and scattering of several atmospheric variables, such as aerosols, traces gases, Rayleigh scattering, water vapor and ozone [38]. To obtain the spectral irradiance, first, SMARTS2 calculate the spectral direct beam ($E_{bn,\lambda}$) as:

$$E_{bn,\lambda} = I_{o,\lambda} \cdot T_{a,\lambda} \cdot T_{w,\lambda} \cdot T_{n,\lambda} \cdot T_{g,\lambda} \cdot T_{O_3,\lambda} \cdot T_{R,\lambda}, \quad (1)$$

where $I_{o,\lambda}$ is the extraterrestrial spectral irradiance and T is the transmittance at each wavelength for aerosols ($T_{a\lambda}$), water vapor ($T_{w,\lambda}$), trace gases ($T_{g,\lambda}$), nitrogen dioxide ($T_{n,\lambda}$), ozone ($T_{O_3,\lambda}$) and Rayleigh scattering ($T_{R,\lambda}$). Then, the spectral diffuse horizontal irradiance is calculated as the sum of the diffuse irradiance due to Rayleigh scattering ($E_{dR,\lambda}$), aerosols ($E_{da,\lambda}$) and backscattering ($E_{db,\lambda}$). This is:

$$E_{d,\lambda} = E_{dR,\lambda} + E_{da,\lambda} + E_{db,\lambda}. \quad (2)$$

Finally, the global horizontal is calculated using $E_{bn,\lambda}$, $E_{d,\lambda}$ and the solar zenith angle θ_z:

$$E_{g,\lambda} = E_{bn,\lambda} \cdot cos(\theta_z) + E_{d,\lambda}. \quad (3)$$

Afterward, SMARTS2 calculates the spectral irradiance for each component between 280 nm and 4000 nm, with a resolution of 0.5 nm between 280 and 400 nm, 1 nm between 400 and 1700 nm and 5 nm between 1700 and 4000 nm. A detailed explanation of each transmittance parametrization can be found in Refs. [37,38].

The model requires different inputs to calculate the spectral solar irradiance. To obtain an accurate transmittance due to aerosols we used the data from AERONET, such as AOD at 500 nm single scattering albedo and the asymmetry factor. We also used different atmospheric measurements such as water vapor, ozone and

concentration of gases to obtain each transmittance due to gases.

A no-AOD case was also created, setting a fixed value for the AOD of 0.05 throughout the entire period. The value chosen was obtained from the time series of AOD, being a typical value for clear sky days in Santiago with no pollution after a rain episode, representative of background conditions.

We also calculated the aerosol radiative forcing (ARF) to quantify the difference between the solar irradiance in normal conditions and the one estimated for the no-AOD case. The ARF is calculated as:

$$ARF = (1-\alpha)\cdot\Delta F_{BOA}, \tag{4}$$

where ΔF_{BOA} is the difference between the irradiance measured and the irradiance calculated with no-AOD.

To validate the model, the MBD (mean bias difference), the RMSD (root mean square deviation) and the MAD (mean absolute difference) defined by Gueymard [39] were used:

$$MBD = (100 / O_m)\left[\sum_{i=1}^{N}(p_i - o_i)\right], \tag{5}$$

$$RMSD = (100/O_m)\left[\sum_{i=1}^{N}\frac{(p_i - o_i)^2}{N}\right]^{1/2}, \tag{6}$$

$$MAD = (100 / O_m)\left[\sum_{i=1}^{N}|p_i - o_i|\right], \tag{7}$$

where O_m is the mean of the observations and o_i and p_i are the observation and the modelled data at the time i.

Finally, in order to obtain a background baseline in which no aerosols are considered, we corrected the values obtained with SMARTS2 using a bias correction technique. Since SMARTS2 tends to overestimate the surface radiation over Santiago on clear skies for the range of observed AOD (MBD of 2.2%, 0.5% and 7.8% for the GHI, DNI and DHI respectively), leaving the model uncorrected would therefore overestimate the effect of aerosols on the surface solar irradiance. For this study, the use of SMARTS2 is solely to create this baseline representative of a no-AOD case and not to attempt to create a realistic simulation of the solar irradiance in the presence of aerosols. Several methods exist to correct models using linear and no-linear methodologies based on measurements [40]. For this study, we corrected SMARTS2 using an additive mean bias correction [41–43], using the MBD calculated from the modelled data and the observations, and adding it to the modelled dataset in the no-AOD case.

3.4. PV power output model

First, the tilted global irradiance (G_{POA}) was calculated to evaluate the effect of aerosols on the power production with different PV technologies using the Klucher model [44]. To calculate G_{POA}, the surface reflectance was set to 0.3 (aged concrete) and the tilt angle was set to 32°. Then, the power output for the different technologies was calculated using the model described by NREL [45]:

$$P_{PV} = P_{STC}\left(\frac{G_{POA}}{G_{STC}}\right)\left(1 - \frac{\delta}{100}\left(T_{cell-avg} - T_{cell}\right)\right), \tag{8}$$

where P_{PV} is the panel power output, P_{STC} is the power in standard test conditions, G_{POA} is the tilted global irradiance, G_{STC} is the reference irradiance, δ is the temperature coefficient for the power and $T_{cell-avg}$-T_{cell} is the average cell temperature minus the cell temperature. To calculate T_{cell} we used the expressions obtained by Kratochvil et al. [46]:

$$T_{cell} = T_m + \frac{G_{POA}}{G_{STC}}\cdot\Delta T_{cnd}, \tag{9}$$

$$T_m = G_{POA}\cdot\exp(a_{PV} + b_{PV}\cdot WS) + T_a, \tag{10}$$

where T_m is the module-back surface temperature, ΔT_{cnd} is the conduction temperature drop, T_a is the ambient temperature, WS is the wind speed, and a_{PV} and b_{PV} are empirical heat transfer coefficients specific for each solar module technology.

We obtained the heat transfer coefficients (a_{PV} and b_{PV}) and the conduction temperature drop from Kratochvil et al. [46]. For the m-Si (a-Si) the coefficients correspond to −3.47 (−3.58), −0.0594 (−0.113) and 3 (3) for the a_{PV}, b_{PV} and ΔT_{cnd} respectively.

For both PV systems (m-Si and a-Si) the losses were estimated to 10%, which account for losses due to degradation (obtained from Urrejola et al. [25]) and the inverter efficiency, which was obtained from the manufacturer. The mismatch factor (MM) was estimated using the model proposed by Caballero et al. [47], which account for spectral losses by aerosols, air mass and water vapor using the following expression:

$$MM = f(AOD)_{PV} + f(AM)_{PV} + f(w)_{PV}, \tag{11}$$

where $f(AOD)_{PV}$, $f(AM)_{PV}$, $f(w)_{PV}$ are empirical equation for each PV technology. In Caballero et al. [47] the extended equations and empirical values can be found in detail.

Then, the PV power output in a hypothetical case of no-AOD was calculated with Eq. (8), using the modelled solar irradiance for the no-AOD case. The PV power output calculated in both cases (current conditions and no-AOD) was then corrected using the mean bias difference between the measurements and the PV power output calculated in normal conditions, adding the bias to the PV power output in both cases. Finally, the energy output for each time step was calculated using the PV power output and the timestep (Δt) as:

$$E_{PV} = P_{PV}\cdot\Delta t. \tag{12}$$

3.5. CPV power output model

The power output of a concentrated photovoltaic module was simulated using the model described by Fernández et al. [48]:

$$\begin{aligned} P_{CPV} &= \frac{P_{STC}}{DNI_{STC}} DNI\cdot(1-\delta(T_{cell} - T_{cell-stc})) \\ &\cdot(1-\varepsilon(AM - AM_u))\cdot\left(1-\phi\left(AOD_{550} - AOD_{550,u}\right)\right), \end{aligned} \tag{13}$$

where DNI_{STC} is the reference direct normal irradiance (1000 W/m^2), T_{cell} and $T_{cell-stc}$ are the cell and the STC cell temperatures respectively, δ is the temperature coefficient for the power, ε is the atmospheric mass coefficient for STC conditions, AM and AM_u are the atmospheric mass and the atmospheric mass threshold (the limit where the power is affected by the atmospheric mass), ϕ is the aerosol optical depth coefficient for STC conditions and $AOD_{550,u}$ is the threshold of the AOD in 550 nm. To obtain the AOD in 550 nm the AOD in 500 nm and 380 nm were used with the approximation proposed by Shettle and Fenn [49]:

$$AOD_{550} = 0.2758\cdot AOD_{380} + 0.35\cdot AOD_{500}, \tag{14}$$

where AOD_{380} and AOD_{500} are the aerosol optical depth at 380 and 500 nm.

To calculate T_{cell}, Fernández et al. [48] propose the following expression:

$$T_{cell} = T_a + a_{CPV} \cdot DNI + b_{CPV} \cdot WS, \quad (15)$$

The coefficients used in this work correspond to the ones used by Fernandez et al. (Tables 1 and 2 in Ref. [48]). Then, the CPV power output in a hypothetical case with no-AOD was calculated using the direct normal irradiance obtained with no-AOD. Finally, the power and energy output calculated in normal condition in Santiago were compared with the no-AOD case.

4. Results and discussions

4.1. Aerosol effects on solar irradiance

The scatter plot in Fig. 6 shows the difference between the irradiance measured and the irradiance obtained with the corrected SMARTS2 model. The model for the global component explains almost all the variance ($R^2 = 0.99$), with a RMSD of 2.5% and a MAD of 1.9%. The goodness of fit obtained is similar to the ones obtained by the models proposed by Xia [50] and Xia [51]. The RMSD (MAD) for the direct and diffuse component is higher than the one for the global component, with a RMSD of 3.6% (2.7%) and 12% (9.2%) respectively. The R^2 obtained for the direct and diffuse component is 0.97 and 0.87 respectively. The MBD used to correct the model correspond to 2.2%, 0.5% and 7.8% for the GHI, DNI and DHI respectively. The RMSD and MAD obtained without the bias correction can also be found in Fig. 6.

The MAD and RMSD obtained are expected and within the range compared to other clear sky solar irradiance models [52]. The differences between the measurements and the model may be caused by the parametrizations used in SMARTS2 to calculate the scattering produced by aerosols and the attenuation of the direct beam component [53].

Fig. 7 shows the annual hourly mean irradiance for the GHI, DNI, DHI and direct horizontal component in clear sky conditions. From this figure, it is clear that the model used to calculate the clear sky irradiance follows closely the solar irradiance measured at any time of the day in Santiago with the current atmospheric conditions.

There is a difference between the case with aerosols and the no-AOD one, more noticeable for the direct and diffuse components rather than the global component. This is consistent with other studies [50,54,55] and is partly due to the partitioning of direct and diffuse irradiance caused by aerosols. Since GHI is the sum of the direct and diffuse horizontal components, the overall reduction of GHI would be mostly associated with the absorption produced by aerosols, as the reduction due to the scattering on the direct horizontal component is compensated by the increase of DHI [11].

Furthermore, the differences between the measurements and the no-AOD case are not symmetric around noon and present more extreme values during the morning rather than the evening. These critical episodes might reduce the GHI and the DNI in more than 20% compared to the same hour but with no aerosols. The overall higher reduction in the morning may be explained by the larger concentration of air pollutants, the larger ventilation in the evening [56], the air mass increase and lower height of the boundary layer at this period [16].

The difference between the seasonal measured irradiance and the irradiance calculated assuming no-AOD is shown in Table 2.

The differences between the measurements and the no-AOD case are greater in autumn for the DNI and DHI components, and can be explained by the larger AOD and the intensification of the attenuation produced by the increase of the solar zenith angle in autumn [57]. The effect of aerosols is larger on the direct and diffuse component (−14.1% and 35.4%) compared to the global component (−3.5%).

One case of interest is winter, where the GHI difference reaches its maximum at the time that the DHI difference reaches its minimum. One reason for this could be that the single scattering albedo reaches a minimum in winter (See Fig. 2). A lower SSA in winter is associated with an increase of the extinction due to absorption and a reduction of the fraction of solar irradiance scattered by aerosols [54,55]. The increase of absorption may be caused by the increase of both wood-burning [17] and aerosols such as black carbon at autumn-winter in Santiago [58].

The results obtained indicate that aerosols present in Santiago tend to disperse more solar irradiance than they absorb, which is a main characteristic of fine particles and dust [13,50]. This is consistent with a recent study by Barraza et al. [30] which found that motor vehicles and industrial sources were the main sources for fine particulate matter in Santiago.

Taking into account the surface reflectance (α) in Santiago [59], it is possible to calculate the aerosol radiative forcing (ARF) for clear skies using Eq. (4). This is shown in Table 3 together with other studies found in the literature. The ARF in Santiago is consistent with locations with similar annual mean AOD, where the differences between them may be explained by the type and the aerosols composition. Thus, aerosol composition may be an important variable over urban environments that should be incorporated in future studies. The results found are in good agreement with ARF on continental background zones shown by García et al. [60] using AERONET data, with values in autumn/winter between $-12\ W/m^2$ and $-29\ W/m^2$.

4.2. Aerosol effects on conventional PV modules

From the previous section, we can see that aerosols produce a significant effect on the different solar irradiance components in Santiago. This change on solar irradiance produced by aerosols can also be translated to a change in the power output for the different solar modules technologies.

As in the previous section, the model used to calculate the PV power output was corrected using the MBD between the observations and the model, which correspond to 1.3% and 4.5% for the m-Si and a-Si respectively. Once again, the bias correction was used to obtain good estimates of the PV power output.

The scatter plots in Fig. 8 shows the difference between the measured and calculated PV power output using the PV model proposed. The R^2 is 0.98 on both cases and the MAD is 5.5% and 5.7% for the m-Si and a-Si respectively. The difference between the PV power output measured and calculated can be traced to three sources: 1) the heat transfer model used to calculate the cell temperature in the different PV technologies which can generate a difference on the solar cell temperature, and hence, on the power output; 2) the solar irradiance model used to calculate the tilted global irradiance, which can overestimate the diffuse component;

Table 2
Difference between the measurements and the no-AOD case for the GHI, DNI and DHI solar irradiance components.

Season	GHI	DNI	DHI
Summer (DJF)	−1.4%	−11.4%	36.3%
Autumn (MMA)	−5.3%	−17.2%	37.4%
Winter (JJA)	−6.0%	−16.3%	31.2%
Spring (SON)	−3.7%	−13.4%	34.3%
Annual	**−3.5%**	**−14.1%**	**35.4%**

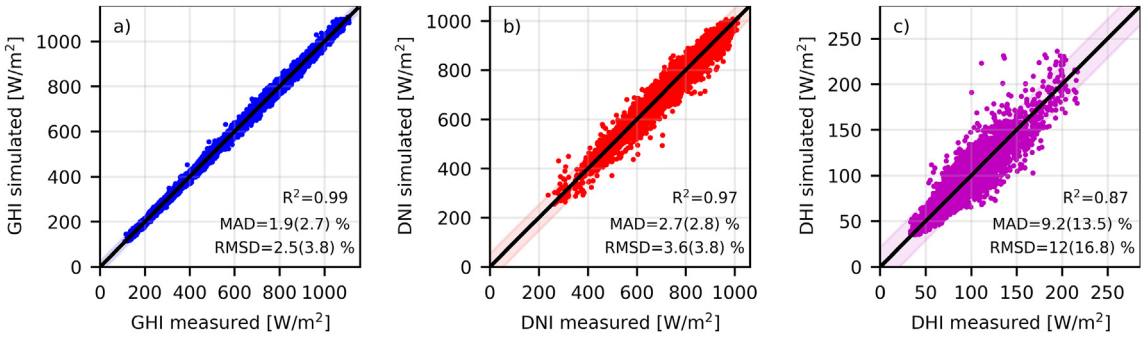

Fig. 6. Scatter plot of a) GHI, b) DNI and c) DHI between the measurements and the irradiance obtained with the SMARTS2 model. The solid black lines represent a 1:1 ratio and the shaded areas represent a confidence interval of 95%. The values in parenthesis correspond to the goodness of fit of the model without the bias correction.

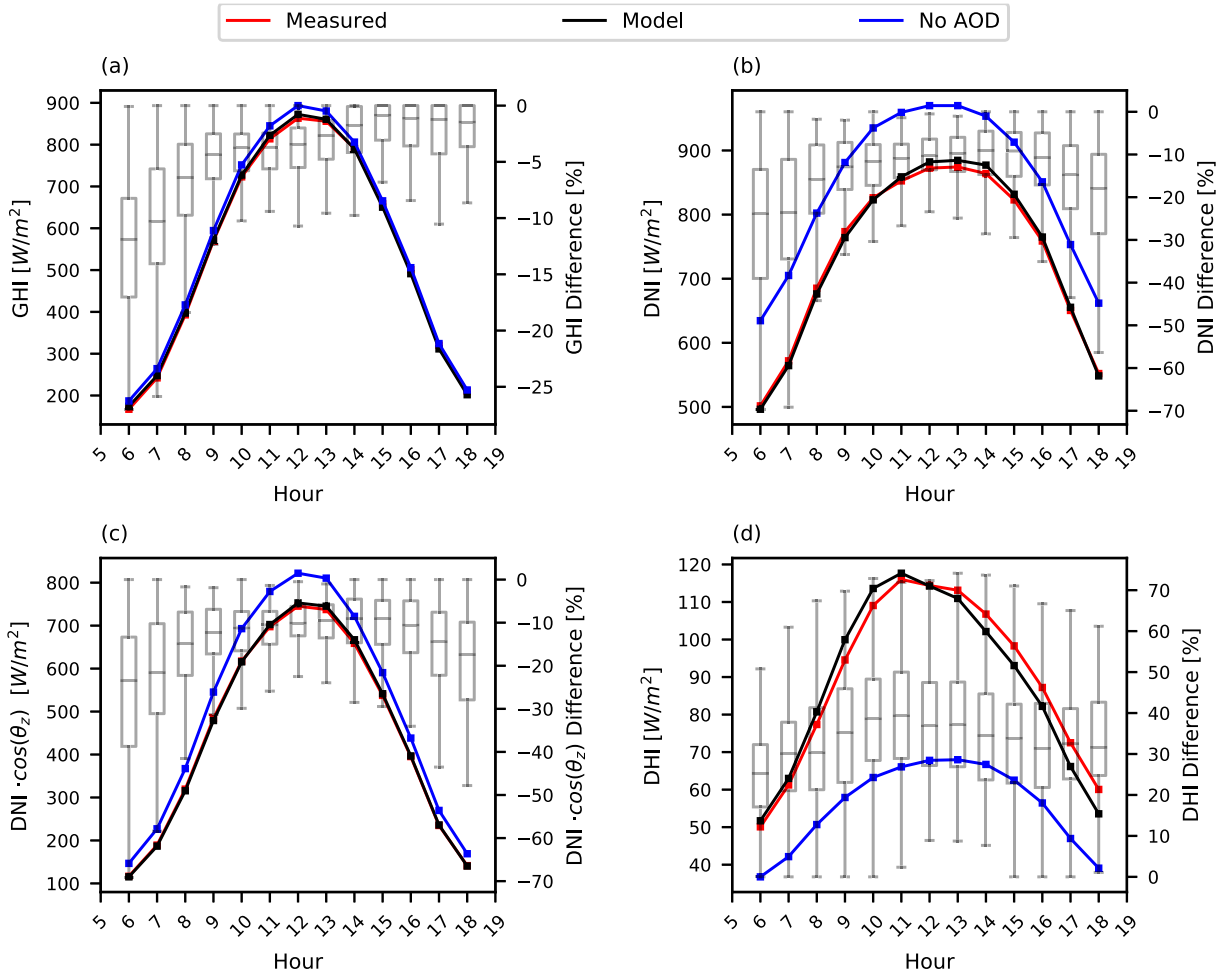

Fig. 7. Annual hourly solar irradiance (left axis) of the measurements, the solar irradiance obtained with the SMARTS model and the no-AOD case for the a) Global horizontal irradiance (GHI), b) the direct normal irradiance (DNI) c) the Direct horizontal irradiance (DNI · cos θ_z) and d) the diffuse horizontal irradiance (DHI). The boxplot (right axis) shows the difference between the measurements and the no-AOD case.

and 3) the effect of soiling which is still present in the measurements.

With the previous results, the power output measured and the calculated with the PV model in normal conditions were compared with the case created with no-AOD. This is shown in Fig. 9, where we can see the difference between the three cases for the 2 types of PV silicon modules. The difference between the power output measured and the power output estimated in a no-AOD case is more significant in the morning than in the evening, which is consistent with the effect of aerosols on the solar irradiance at the same hours (See Fig. 7).

Fig. 10 shows the boxplot for 1) the monthly difference between the measurements and the no-AOD case; and 2) the hourly MM. As the difference between the measurements and the no-AOD case shows, there is a similar pattern to the effect of aerosols on the solar irradiance, with higher differences between April and September.

Table 3
Annual mean AOD and ARF in Santiago and other locations found in the literature.

Location	Reference	AOD mean	ARF [W/m^2]
Santiago, Chile	In this study	0.20	−26
São Paulo, Brazil	Yamasoe et al [61]	0.18	−20
Valencia, Spain	Esteve et al [62]	0.19	−17
Karashi, Pakistan	Bibi et al [63]	0.28	−37
Tainan, Taiwan	Chou et al [64]	0.73	−39
Xianghe, China	Xia et al [11]	0.82	−33

Looking at the monthly MM for both technologies, is clear that the a-Si technology presents a higher spectral mismatch compared to the m-Si; and hence, the higher difference appreciated in the a-Si. This higher MM may be caused by the spectral response of the a-Si technology, located near the visible range of the solar spectrum, which is sensible to atmospheric mass changes and the effect of aerosols. The impact of aerosols on the production of a-Si modules has been explained by different studies that show the PV modules sensitivity to changes in AOD [65,66].

After analyzing the PV power output, we calculated the energy output for the different PV technologies using Eq. (12). We found differences of −2.7%, −10.4%, −11.2% and −8.3% for the m-Si technology and differences of −3.9%, −9.9%, −11.7% and −10.5% for the a-Si technology in summer, autumn, winter and spring respectively. We also found an annual difference of −7.2% and −8.7% for the m-Si and a-Si respectively. The maximum decrease in winter can be attributed to changes of aerosols types, the increase of atmospheric mass, the larger concentration of air pollutants and the low height of the boundary layer. Moreover, the a-Si technology presents a slightly higher loss in comparison with the m-Si modules.

We note that the effect of aerosols on the PV energy output is larger than the effect on the global horizontal irradiance. One explanation could be soiling, which decreases the PV power output

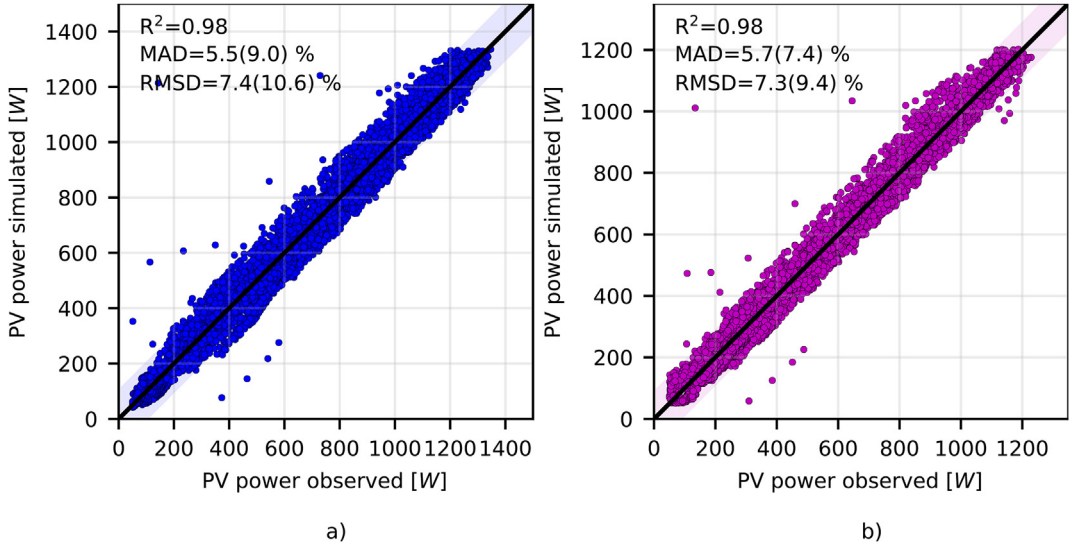

Fig. 8. PV power output measured and calculated with the PV model for a) m-Si and b) a-Si modules. The black line represents a 1:1 ratio and the shaded area correspond to a confidence interval of 95%. The values in parenthesis correspond to the goodness of fit without the model corrected by bias.

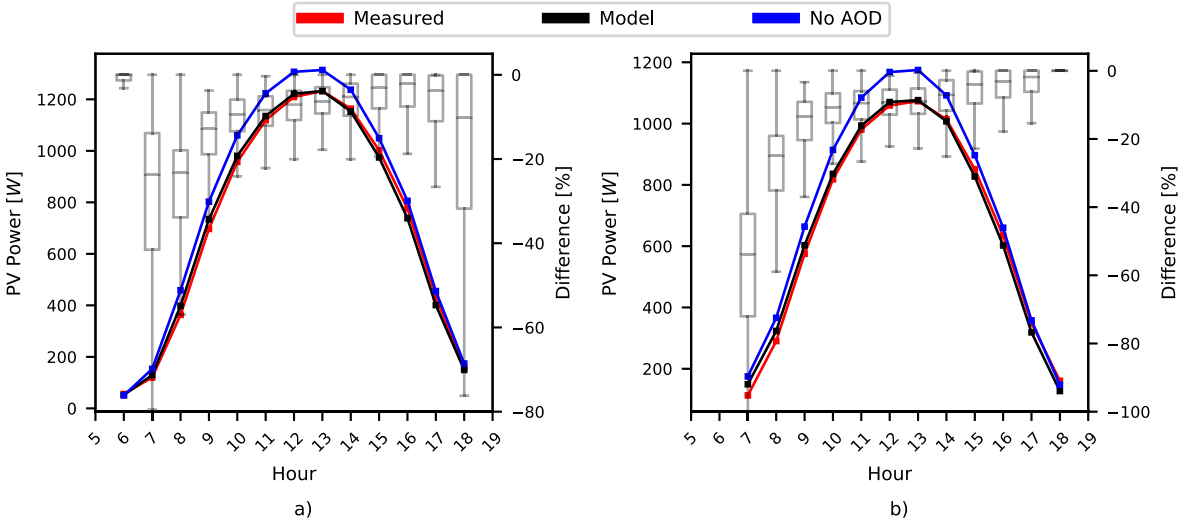

Fig. 9. Annual hourly PV power output measured (left axis), obtained with the PV model and estimated without AOD through the year for a) m-Si and b) a-Si modules. The boxplot shows the hourly difference between the measurements and the no-AOD case (right axis).

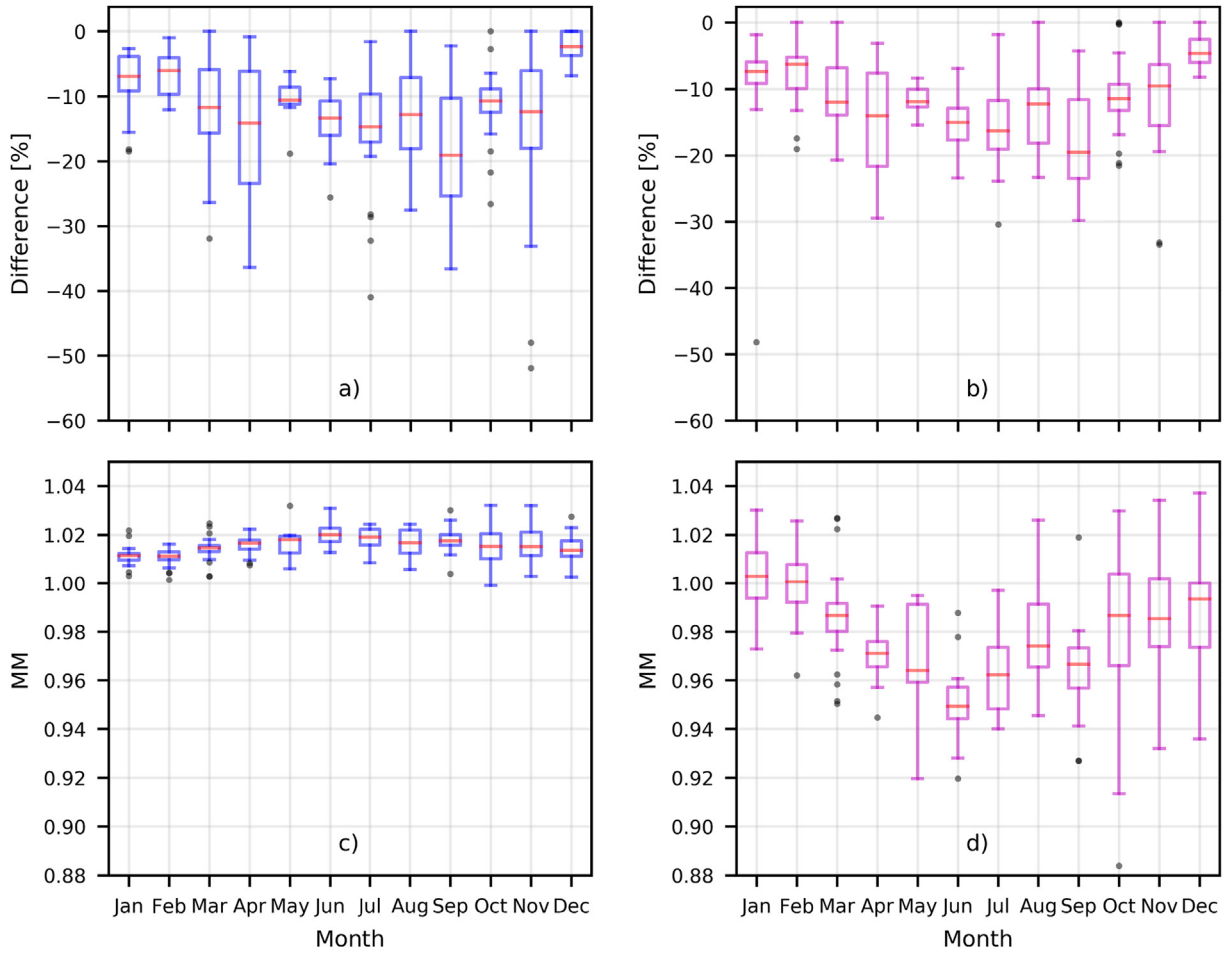

Fig. 10. At the top, the boxplot for the hourly difference between the power output measured and the no-AOD case for the a) m-Si and the b) a-Si modules. At the bottom, the hourly MM estimated for the c) m-Si and the d) a-Si technology.

measured compared to the modelled, especially when the PV modules were not cleaned for several days. Moreover, soiling is not modelled and it is expected to be lower in the no-AOD case compared to reality, as fewer particles would be deposited on the solar modules, increasing the PV energy output.

Although the effect of soiling is present, it is correct to say that the effect of aerosols (and only aerosols) on PV power output is quite similar to the one obtained for the GHI as a first-order approximation, which is not far from the results previously found in this study for the effect of aerosols on the solar irradiance.

4.3. Aerosol effects on CPV modules

A similar analysis can be done for the CPV technology. Fig. 11 shows the difference between the power output obtained with the current conditions and the one obtained with no-AOD using Eq. (13). The seasonal variation shown in this Figure can be explained by: 1) the dependence of the CPV technology on the DNI and the effect of aerosols on the distribution of DNI and DHI [67] ; 2) the scattering/absorption produced by aerosols in certain wavelengths.

The higher differences found in April could be related to days in 2016 with high AOD values (over 0.4), which impacted heavily on the PV power output on those days.

In general, aerosols have a higher influence in wavelengths near the visible spectrum than in the near-infrared, and thus, AOD has a higher effect on the top sub cell of a multi junction solar cell, which has a spectral response near the visible spectrum [68].

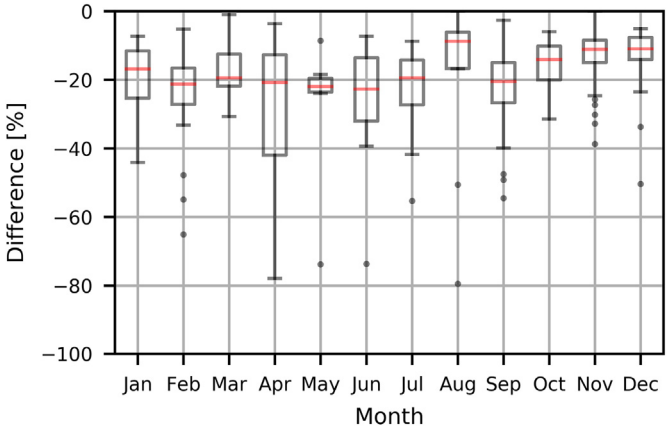

Fig. 11. Monthly boxplot, based on daily means, for the difference between the power output calculated with the current conditions and the one obtained with no-AOD for the CPV technology throughout the year.

To obtain the difference between the energy output in normal condition and the energy output in the no-AOD case, we calculated the energy output using Eq. (12). The annual difference for this technology is −16.4%, with seasonal differences of −15.8%, −19.2%, −16.9% and −14.4% for summer, autumn, winter

and spring respectively. The maximum decrease found in autumn is much higher than the difference found for conventional silicon modules. The difference between the effect of aerosols on the CPV and the conventional technologies may be caused by the stronger effect of aerosols on the direct irradiance component. Power output losses caused by aerosols found by Chan et al. [69], obtained with measurements and a custom model in locations with similar atmospheric conditions (annual mean AOD between 0.15 and 0.25 and w near 1.2 cm), were close to −16%, quite similar to the result obtained in this study.

Although the obtained effect of aerosols on the CPV energy output is important, we cannot validate these results with in-situ measurements as we did with the conventional solar modules, due to the unavailability of this technology in the time period of the study.

5. Conclusions

This study presented the effect of aerosols on the solar irradiance and PV power output for different technologies in Santiago, using the SMARTS2 model, AERONET data and other atmospheric measurements.

Using SMARTS2, the estimated annual differences between the actual condition in Santiago and the no-AOD case in clear sky days are −3.5%, −14.1% and +35.4% for the GHI, DNI and DHI respectively.

The results obtained with the SMARTS2 model were also used to calculate the PV power output for two technologies (m-Si and a-Si) and estimated the effect of aerosols on the PV power and energy output in Santiago. The results show a difference in the energy output between the actual conditions and the no-AOD case of −7.2% and −8.7% for the m-Si and a-Si respectively, with a maximum decrease in the winter season between −11.2% and −11.7%. We note that the difference found in the PV power output between the current conditions and the no-AOD case includes the effect of soiling, as the PV modules were not cleaned daily. However, as a first order approximation, the effect of aerosols on the PV power output should be closely related to the global horizontal irradiance losses due to aerosols. The mismatch factor estimated shows that aerosols could have a larger impact on the a-Si module compared to the m-Si module. A new study in which the solar panels are cleaned regularly is required to effectively filter out the effect of soiling.

Although there are some studies where the effect of aerosols on the PV energy output is larger (eg. Refs. [14,24]), the results presented here show a significant effect that cannot be neglected in the design of photovoltaic plants or for the development of solar forecasting tools.

The solar irradiance model was also used to estimate the effect of aerosols on the energy output of a CPV system. The annual difference between the actual condition and the no-AOD case is −16.4%, showing that this technology is the most sensitive to aerosols.

Future studies could focus on: the effect of aerosols in the solar spectrum and the PV spectral response in Santiago to get a proper estimation on the power output for the different PV technologies; the spatial distribution and type of aerosols in Santiago, to obtain a proper estimation that is representative of the whole city [70]; and the economic negative externalities of air pollution due to the decrease in surface solar irradiance for Santiago, which could improve the estimation and economic projections of different solar energy projects in Santiago as well as promote policies that could reduce the fine particulate matter.

Acknowledgments

The research has received financing from the Center for Climate and Resilience Research (FONDAP 15110009), the project “Black Carbon in the Andean Cryosphere” (CONICYT-ANILLOS ACT1410) and the grant CONICYT-PFCHA/MagísterNacional/2017-22170934.

Nomenclature

α	Surface reflectance [dimensionless]
β	Tilt angle [$^\circ$]
ΔF_{BOA}	Difference between the irradiance measured and the estimated without aerosols [W/m^2]
ΔT_{cnd}	Conduction temperature drop [$^\circ$C]
δ	Temperature coefficient for the power [1/$^\circ$ C.]
ε	Atmospheric mass coefficient for STC condition = 0.041 [dimensionless]
θ_z	Solar zenith angle [$^\circ$]
ϕ	Aerosol optical depth coefficient for STC condition = 0.32 [dimensionless]
AM	Atmospheric mass [dimensionless]
AM_u	Atmospheric mass threshold = 2.1
AOD	Aerosol optical depth [dimensionless]
$AOD_{550,u}$	Threshold of the AOD at 550 nm = 0.25
AOD_{550}	AOD at 550 nm [dimensionless]
ARF	Aerosol radiative forcing [W/m^2]
CPV	Concentrating photovoltaic
DHI	Diffuse normal irradiance [W/m^2]
DNI	Direct normal irradiance [W/m^2]
DNI_{STC}	Direct normal irradiance at standart test condition, 1000 W/m^2
$E_{bn,\lambda}$	Spectral direct beam irradiance [W/m·2 nm]
$E_{d,\lambda}$	Spectral diffuse horizontal irradiance [W/m·2 nm]
$E_{g,\lambda}$	Spectral global horizontal irradiance [W/m·2 nm]
E_{PV}	PV energy output [kWh]
G_{POA}	Global tilted irradiance [W/m^2]
G_{STC}	Direct normal irradiance at standart test condition, 1000 W/m^2
G_{STC}	Global irradiance at standart test condition, 1000 W/m^2
GHI	Global horizontal irradiance [W/m^2]
$I_{o,\lambda}$	Extraterrestrial solar irradiance [W/m·2 nm]
I_{SC}	Solar constant, 1360 W/m^2
m_a	Aerosol optical mass [dimensionless]
MM	Mismatch factor [dimensionless]
P_{CPV}	PV Power output [W]
P_{PV}	PV Power output [W]
P_{STC}	Power output at standart test conditions [W]
PV	Photovoltaic
SSA	Single scattering albedo [dimensionless]
T_m	Module-back surface temperature [$^\circ$C]
$T_{a,\lambda}$	Spectral transmitance due to aerosols [dimensionless]
T_a	Ambient temperature [$^\circ$C]
$T_{cell-avg}$	Average photovoltaic cell temperature [$^\circ$C]
$T_{cell-stc}$	Photovoltaic cell temperature at standart test condition = 25°C
T_{cell}	Photovoltaic cell temperature [$^\circ$C]
$T_{g,\lambda}$	Spectral transmitance due to nitrogen dioxide [dimensionless]
$T_{n,\lambda}$	Spectral transmitance due to trace gases [dimensionless]
$T_{O_3,\lambda}$	Spectral transmitance due to ozone [dimensionless]
$T_{R,\lambda}$	Spectral transmitance due to Rayleight scattering [dimensionless]
$T_{w,\lambda}$	Spectral transmitance due to water vapor [dimensionless]

w	Water vapor [cm]
WS	Wind speed [m/s]
MAD	Mean absolute difference
MBD	Mean bias difference
RMSD	Root mean square deviation

References

[1] Ministerio de Energia, Energia 2050, 2015. www.energia2050.cl/wp-content/uploads/2016/08/Energy-2050-Chile-s-Energy-Policy.pdf.

[2] R. Rondanelli, A. Molina, M. Falvey, The Atacama surface solar maximum, Bull. Am. Meteorol. Soc. 96 (3) (2015) 405–418, https://doi.org/10.1175/BAMS-D-13-00175.1. ISSN 00030007, doi:\let\@tempa\bibinfo@X@.

[3] R.A. Escobar, C. Cortes, A. Pino, E.B. Pereira, F.R. Martins, J.M. Cardemil, Solar energy resource assessment in Chile: satellite estimation and ground station measurements, Renew. Energy 71 (2014) 324332, https://doi.org/10.1016/j.renene. 2014.05.013. ISSN 09601481, doi:\let\@tempa\bibinfo@X@, http://linkinghub.elsevier.com/retrieve/pii/S096014811400264X.

[4] R.A. Escobar, C. Cortés, A. Pino, M. Salgado, E.B. Pereira, F.R. Martins, J. Boland, J.M. Cardemil, Estimating the potential for solar energy utilization in Chile by satellite-derived data and ground station measurements, Sol. Energy 121 (2015) 139–151, https://doi.org/10.1016/j.solener.2015.08.034. ISSN 0038092X, doi:\let\@tempa\bibinfo@X@.

[5] G. Ramírez-Sagner, C. Mata-Torres, A. Pino, R.A. Escobar, Economic feasibility of residential and commercial PV technology: the Chilean case, Renew. Energy 111 (2017) 332–343, https://doi.org/10.1016/J.RENENE. 2017. 04.011. ISSN 0960-1481, doi:\let\@tempa\bibinfo@X@, https://www.sciencedirect.com/science/article/pii/S0960148117303166.

[6] P. Campos, L. Troncoso, P.D. Lund, C. Cuevas, A. Fissore, R. Garcia, Potential of distributed photovoltaics in urban Chile, Sol. Energy 135 (2016) 43–49, https://doi.org/10.1016/j.solener.2016.05.043, 10.1016/j.solener.2016.05.043, ISSN 0038092X, doi:\let\@tempa\bibinfo@X@.

[7] A. Zurita, A. Castillejo-Cuberos, M. García, C. Mata-Torres, Y. Simsek, R. García, F. Antonanzas-Torres, R.A. Escobar, State of the Art and Future Prospects for Solar PV Development in Chile, 2018, https://doi.org/10.1016/j.rser.2018.04.096 doi:\let\@tempa\ bibinfo@X@, https://linkinghub.elsevier.com/retrieve/pii/S1364032118303198.

[8] IRENA, The Power to Change: Solar and Wind Cost Reduction Potential to 2025, June, 2016. ISBN 9789295111974.

[9] ITA, 2016 Top markets report renewable energy, country case study : Chile, Tech. Rep, ITA, 2016, pp. 31–35.

[10] J. Haas, R. Palma-Behnke, F. Valencia, P. Araya, G. Diaz- Ferran, T. Telsnig, L. Eltrop, M. Diaz, S. Puschel, M. Grandel, R. Roman, G. Jimenez-Estevez, Sunset or sunrise? Understanding the barriers and options for the massive deployment of solar technologies in Chile, Energy Policy 112 (2018) 399–414, https://doi.org/10.1016/j.enpol. 2017. 10.001. ISSN 03014215, doi:\let\@tempa\bibinfo@X@, https://www.sciencedirect.com/science/article/pii/S0301421517306249.

[11] X. Xia, Z. Li, P. Wang, H. Chen, M. Cribb, Estimation of aerosol effects on surface irradiance based on measurements and radiative transfer model simulations in northern China, J. Geophys. Res. Atmosphere 112 (22) (2007), https://doi.org/10.1029/2006JD008337. D22S10, ISSN 01480227, doi:\let\@tempa\bibinfo@X@doi10.1029/2006JD008337.

[12] K.D. Kanniah, J. Beringer, N.J. Tapper, C.N. Long, Aerosols and their influence on radiation partitioning and savanna productivity in northern Australia, Theor. Appl. Climatol. 100 (3) (2010) 423–438, https://doi.org/10.1007/s00704-009-0192-z. ISSN 0177798X, doi:\let\@tempa\bibinfo@X@, http://link.springer.com/10.1007/s00704-009-0192-z.

[13] I. Foyo-Moreno, I. Alados, M. Antan, J. Fernandez-Galvez, A. Cazorla, L. Alados-Arboledas, Estimating aerosol characteristics from solar irra- diance measurements at an urban location in Southeastern Spain, J. Geophys. Res. 119 (4) (2014) 1845–1859, https://doi.org/10.1002/2013JD020599. ISSN 21562202, doi:\let\@tempa\bibinfo@X@doi10.1002/2013JD020599.

[14] X. Li, F. Wagner, W. Peng, J. Yang, D.L. Mauzerall, Reduction of solar photovoltaic resources due to air pollution in China, Proc. Natl. Acad. Sci. 114 (45) (2017) 11867–11872, https://doi.org/10.1073/pnas.1711462114. ISSN 00278424, doi:\let\@tempa\bibinfo@X@, http://www.pnas.org/lookup/doi/10.1073/pnas.1711462114.

[15] J. Rutllant, R. Garreaud, Meteorological air pollution potential for Santiago, Chile: towards an objective episode forecasting, Environ. Monit. Assess. 34 (3) (1995) 223–244, https://doi.org/10.1007/BF00554796. ISSN 01676369, doi:\let\@tempa\bibinfo@X@.

[16] R.C. Muñoz, A.A. Undurraga, Daytime mixed layer over the Santiago Basin: description of two years of observations with a lidar ceilome- ter, J. Appl. Meteorol. Climatol. 49 (8) (2010) 1728–1741, https://doi.org/10.1175/2010JAMC2347.1. ISSN 15588424, doi:\let\@tempa\bibinfo@X@.

[17] M. Mena-Carrasco, E. Oliva, P. Saide, S.N. Spak, C. de la Maza, M. Osses, S. Tolvett, J.E. Campbell, T.e.C.C. Tsao, L.T. Molina, Estimating the health benefits from natural gas use in transport and heating in Santiago, Chile, Sci. Total Environ. 429 (2012) 257–265, https://doi.org/10.1016/j.scitotenv.2012.04.037. ISSN 00489697, doi:\let\@tempa\bibinfo@X@.

[18] J. Escribano, L. Gallardo, R. Rondanelli, Y.S. Choi, Satellite retrievals of aerosol optical depth over a subtropical urban area: the role of stratification and surface reflectance, Aerosol Air Qual. Res. 14 (3) (2014) 596–607, https://doi.org/10.4209/aaqr.2013.03.0082. ISSN 20711409, doi:\let\@tempa\bibinfo@X@.

[19] L. Gallardo, F. Barraza, A. Ceballos, M. Galleguillos, N. Huneeus, F. Lambert, C. Ibarra, M. Munizaga, R. O'Ryan, M. Osses, S. Tol- vett, A. Urquiza, K.D. Veliz, Evolution of air quality in Santiago: the role of mobility and lessons from the science-policy interface, Elem Sci Anth 6 (1) (2018) 38, https://doi.org/10.1525/elementa.293. ISSN 2325-1026, doi:\let\@tempa\bibinfo@X@, https://www.elementascience.org/article/10.1525/elementa.293/.

[20] R.R. Cordero, G. Seckmeyer, A. Damiani, J. Jorquera, J. Carrasco, R. Munoz, L. Da Silva, F. Labbe, D. Laroze, Aerosol effects on the UV irradiance in Santiago de Chile, Atmos. Res. 149 (November) (2014) 282–291, https://doi.org/10.1016/j.atmosres.2014.07.002, 10.1016/j.atmosres.2014.07.002, ISSN 01698095, doi:\let\@tempa\ bibinfo@X@.

[21] A. Molina, Un modelo semi-empirico para la radiacion solar en Chile, Master's Thesis, Universidad de Chile (2012) 1–32.

[22] A. Molina, M. Falvey, R. Rondanelli, A solar radiation database for Chile, Sci. Rep. 7(1), ISSN 20452322, doi:\let\@tempa\ bibinfo@X@doi10.1038/s41598-017-13761-x.

[23] D. Calinoiu, M. Paulescu, I. Ionel, N. Stefu, N. Pop, R. Boata, A. Pacu- rar, P. Gravila, E. Paulescu, G. Trif-Tordai, Influence of aerosols pollution on the amount of collectable solar energy, Energy Convers. Manag. 70 (2013) 76–82, https://doi.org/10.1016/j.enconman.2013.02.012. ISSN 01968904, doi:\let\@tempa\bibinfo@X@, http://linkinghub.elsevier.com/retrieve/pii/S0196890413001039.

[24] M.H. Bergin, C. Ghoroi, D. Dixit, J.J. Schauer, D.T. Shindell, Large reductions in solar energy production due to dust and particulate air pollution, Environ. Sci. Technol. Lett. 4 (8) (2017) 339–344, https://doi.org/10.1021/acs.estlett.7b00197. ISSN 23288930, doi:\let\@tempa\bibinfo@X@, http://pubs.acs.org/doi/pdf/10.1021/acs. estlett.7b00197.

[25] E. Urrejola, J. Antonanzas, P. Ayala, M. Salgado, G. Ramirez-Sagner, C. Cortes, A. Pino, R. Escobar, Effect of soiling and sunlight exposure on the performance ratio of photovoltaic technologies in Santiago, Chile, Energy Convers. Manag. 114 (2016) 338–347, https://doi.org/10.1016/j.enconman. 2016.02.016. ISSN 01968904, doi:\let\@tempa\bibinfo@X@.

[26] A. Massi Pavan, A. Tessarolo, N. Barbini, A. Mellit, V. Lughi, The effect of manufacturing mismatch on energy production for large- scale photovoltaic plants, Solar Energy 117 (5) (2015) 282–289, https://doi.org/10.1016/j.solener.2015.05.003. ISSN 0038092X, doi:\let\@tempa\bibinfo@X@, https://www.sciencedirect.com/science/article/pii/S0038092X11000892.

[27] H. Pedersen, J. Strauss, J. Selj, Effect of soiling on photovoltaic modules in Norway, Energy Procedia 92 (2016) 585–589, https://doi.org/10.1016/j.egypro.2016.07.023. ISSN 18766102, doi: \let\@tempa\bibinfo@X@.

[28] F.A. Mejia, J. Kleissl, Soiling losses for solar photovoltaic systems in California, Sol. Energy 95 (2013) 357–363, https://doi.org/10.1016/j.solener.2013.06.028. ISSN 0038092X, doi:\let\@tempa\bibinfo@X@, https://www.sciencedirect.com/science/article/pii/S0038092X13002582.

[29] E. Fuentealba, P. Ferrada, F. Araya, A. Marzo, C. Parrado, C. Portillo, Photovoltaic performance and LCoE comparison at the coastal zone of the Atacama Desert, Chile, Energy Convers. Manag. 95 (2015) 181–186, https://doi.org/10.1016/j.enconman.2015.02.036. ISSN 01968904, doi:\let\@tempa\bibinfo@X@.

[30] F. Barraza, F. Lambert, H. Jorquera, A.M. Villalobos, L. Gallardo, Temporal evolution of main ambient PM2.5 sources in Santiago, Chile, from 1998 to 2012, Atmos. Chem. Phys. 17 (16) (2017) 10093–10107, https://doi.org/10.5194/acp-17-10093-2017. ISSN 16807324, doi:\let\@tempa\bibinfo@X@, https://www.atmos-chem-phys.net/17/10093/2017/.

[31] R.G. Rojas, N. Alvarado, J. Boland, R. Escobar, A. Castillejo-Cuberos, Diffuse fraction estimation using the BRL model and relationship of pre-dictors under Chilean, Costa Rican and Australian climatic conditions, Renew. Energy 136 (2019) 1091–1106, https://doi.org/10.1016/j.renene.2018.09.079. ISSN 18790682, doi:\let\@tempa\bibinfo@X@, https://linkinghub.elsevier.com/retrieve/pii/S0960148118311534.

[32] B.N. Holben, T.F. Eck, I. Slutsker, D. Tanre, J.P. Buis, A. Setzer, E. Vermote, J.A. Reagan, Y.J. Kaufman, T. Nakajima, F. Lavenu, I. Jankowiak, A. Smirnov, AERONET - a federated instrument network and data archive for aerosol characterization, Remote Sens. Environ. 66 (1) (1998) 1–16, https://doi.org/10.1016/S0034-4257(98) 00031–00035. ISSN 00344257, doi:\let\@tempa\bibinfo@X@.

[33] M.J. Reno, C.W. Hansen, Identification of periods of clear sky irradiance in time series of GHI measurements, Renew. Energy 90 (2016) 520–531, https://doi.org/10.1016/j.renene.2015.12.031. ISSN 18790682, doi:, nletn@tempan-bibinfo@X@.

[34] W.F. Holmgren, C.W. Hansen, M.A. Mikofski, Pvlib python: a python package for modeling solar energy systems, J. Open Source Softwa 3 (29) (2018) 884, https://doi.org/10.21105/joss.00884, 10.21105/joss.00884, doi:\let\@tempa\bibinfo@X@.

[35] P. Ineichen, A broadband simplified version of the Solis clear sky model, Sol. Energy 82 (8) (2008) 758–762, https://doi.org/10.1016/j.solener.2008.02.009. ISSN 0038092X, doi:\let\@tempa\bibinfo@X@, https://www.sciencedirect.com/science/article/pii/S0038092X08000406.

[36] V.S. Martins, A. Lyapustin, L.A. De Carvalho, C.C. Barbosa, E.M. Novo, Validation of high-resolution MAIAC aerosol product over South America, J. Geophys. Res. 122 (14) (2017) 7537–7559, https://doi.org/10.1002/2016JD026301. ISSN

21562202, doi:\let\@tempa\bibinfo@X@doi10.1002/2016JD026301.
[37] C.A. Gueymard, SMARTS2: a simple model of the atmospheric radiative transfer of sunshine: algorithms and performance assessment, Report No. FSEC-PF-270-95, http://www.fsec.ucf.edu/en/publications/pdf/fsec-pf-270-95.pdf, 1995, 1-84.
[38] C.A. Gueymard, Parameterized transmittance model for direct beam and circumsolar spectral irradiance, Sol. Energy 71 (5) (2001) 325–346, https://doi.org/10.1016/S0038-092X(01)00054-8. ISSN 0038092X, doi:\let\@tempa\bibinfo@X@, https://www.sciencedirect.com/science/article/pii/S0038092X01000548.
[39] C.A. Gueymard, A review of validation methodologies and statistical performance indicators for modeled solar radiation data:Towards a better bankability of solar projects, Renew. Sustain. Energy Rev. 39 (2014) 1024–1034, https://doi.org/10.1016/J.RSER.2014.07.117. ISSN 1364-0321, doi:\let\@tempa\bibinfo@X@, https://www.sciencedirect.com/science/article/pii/S1364032114005693.
[40] J. Polo, S. Wilbert, J.A. Ruiz-Arias, R. Meyer, C. Gueymard, M. Suri, L. Martin, T. Mieslinger, P. Blanc, I. Grant, J. Boland, P. Ineichen, J. Remund, R. Escobar, A. Troccoli, M. Sengupta, K.P. Nielsen, D. Renne, N. Geuder, T. Cebecauer, Preliminary survey on site-adaptation techniques for satellite-derived and reanalysis solar radiation datasets, Sol. Energy 132 (2016) 25–37, https://doi.org/10.1016/j.solener.2016.03.001. ISSN 0038092X, doi:\let\@tempa\bibinfo@X@doi10. @tempa\bibinfo@X@, https://linkinghub.elsevier.com/retrieve/pii/S0038092X16001754.
[41] M. Journée, C. Bertrand, Improving the spatio-temporal distribution of surface solar radiation data by merging ground and satel-lite measurements, Remote Sens. Environ. 114 (11) (2010) 2692–2704. ISSN 0034-4257, doi:\let\@tempa\bibinfo@X@doi10.J.RSE.2010.06.010, https://www.sciencedirect.com/science/article/pii/S0034425710002002.
[42] C.K. Ho, D.B. Stephenson, M. Collins, C.A.T. Ferro, S.J. Brown, Calibration strategies a source of additional uncertainty in climate change projections, Bull. Am. Meteorol. Soc. 93 (1) (2012) 21–26, https://doi.org/10.1175/2011BAMS3110.1. ISSN 00030007, doi:\let\@tempa\bibinfo@X@, https://journals.ametsoc.org/doi/pdf/10.1175/2011BAMS3110.1.
[43] E. Hawkins, T.M. Osborne, C.K. Ho, A.J. Challinor, Calibration and bias correction of climate projections for crop modelling: an idealised case study over Europe, Agric. For. Meteorol. 170 (2013) 19–31, https://doi.org/10.1016/j.agrformet.2012.04.007. ISSN 01681923, doi:\let\@tempa\bibinfo@X@, https://linkinghub.elsevier.com/retrieve/pii/S0168192312001372.
[44] T.M. Klucher, Evaluation of models to predict insolation on tilted surfaces, Sol. Energy 23 (2) (1979) 111–114, https://doi.org/10.1016/0038-092X(79)90110-5. ISSN 0038092X, doi:\let\ @tempa\bibinfo@X@, http://linkinghub.elsevier.com/retrieve/pii/0038092X79901105.
[45] T. Dierauf, A. Growitz, S. Kurtz, C. Hansen, Weather-Corrected Performance Ratio, NREL Technical Report NREL/TP-5200-57991 (April), 2013, pp. 1–16. http://www.nrel.gov/docs/fy13osti/57991.pdf.
[46] J.A. Kratochvil, W.E. Boyson, D.L. King, Photovoltaic array performance model., 2004, https://doi.org/10.2172/919131. Tech. Rep., doi:\let\@tempa\bibinfo@X@.
[47] J.A. Caballero, E.F. Fernandez, M. Theristis, F. Almonacid, G. No- fuentes, spectral corrections based on air mass, aerosol optical depth, and precipitable water for PV performance modeling, IEEE J. Photovolt. 8 (2) (2018) 552–558, https://doi.org/10.1109/JPH0T0V.2017.2787019. ISSN 2156-3381, doi:\let\@tempa\bibinfo@X@, http://ieeexplore.ieee.org/document/8254355/.
[48] E.F. Fernandez, F. Almonacid, T.K. Mallick, P. Perez-Higueras, Analytical modelling of high concentrator photovoltaic modules based on atmospheric parameters, Int. J. Photoenergy 2015 (2015) 1–8, https://doi.org/10.1155/2015/872163. ISSN 1110-662X, doi:\let\@tempa\bibinfo@X@, http://www.hindawi.com/journals/ijp/2015/872163/.
[49] E.P. Shettle, R.W. Fenn, Models of aerosols of lower troposphere and the effect of humidity variations on their optical properties, in: Report AFGL -TR-79-0214, Air Force Geophysics Laboratory, Hanscom, MA, 1979.
[50] X. Xia, A critical assessment of direct radiative effects of different aerosol types on surface global radiation and its components, J. Quant. Spectrosc. Radiat. Transf. 149 (2014) 72–80, https://doi.org/10.1016/j.jqsrt. 2014.07.020. ISSN 00224073, doi:\let\@tempa\bibinfo@X@, http://linkinghub.elsevier.com/retrieve/pii/S0022407314003264.
[51] X. Xia, Parameterization of clear-sky surface irradiance and its implications for estimation of aerosol direct radiative effect and aerosol optical depth, Sci. Rep. 5 (2015) 14376, https://doi.org/10.1038/srep14376. ISSN 20452322, doi:\let\@tempa\bibinfo@X@.
[52] C.A. Gueymard, Clear-sky Irradiance Predictions for Solar Resource Mapping and Large-Scale Applications: Improved Validation Methodology and Detailed Performance Analysis of 18 Broadband Radiative Models, 2012, https://doi.org/10.1016/j.solener. 2011.11.011 doi: \let\@tempa\bibinfo@X@, https://linkinghub.elsevier.com/retrieve/pii/S0038092X11004221.
[53] D.G. Kaskaoutis, H.D. Kambezidis, The role of aerosol models of the SMARTS code in predicting the spectral direct-beam irradiance in an urban area, Renew. Energy 33 (7) (2008) 1532–1543, https://doi.org/10.1016/j.renene.2007.09.006. ISSN 09601481, doi:\let\@tempa\bibinfo@X@, https://www.sciencedirect.com/science/article/pii/S0960148107002777{#}aep-section-id25.
[54] A.F. Bais, A. Kazantzidis, S. Kazadzis, D.S. Balis, C.S. Zerefos, C. Meleti, Deriving an effective aerosol single scattering albedo from spectral surface UV irradiance measurements, Atmos. Environ. 39 (6) (2005) 1093–1102, https://doi.org/10.1016/j.atmosenv.2004.09.080. ISSN 13522310, doi:\let\@tempa\bibinfo@X@, https://linkinghub.elsevier.com/retrieve/pii/S1352231004010246.
[55] D.G. Kaskaoutis, H.D. Kambezidis, Z. Toth, Investigation about the dependence of spectral diffuse-to-direct-beam irradiance ratio on atmospheric turbidity and solar zenith angle, Theor. Appl. Climatol. 89 (3–4) (2007) 245–256, https://doi.org/10.1007/s00704-006-0222-z. ISSN 14344483, doi:\let\@tempa\bibinfo@X@, https://link.springer.com/content/pdf/10.1007{%}2Fs00704-006-0222-z.pdf.
[56] R. Schmitz, Modelling of air pollution dispersion in Santiago de Chile, Atmos. Environ. 39 (11) (2005) 2035–2047, https://doi.org/10.1016/j.atmosenv.2004.12.033. ISSN 13522310, doi:\let\@tempa\bibinfo@X@, https://linkinghub.elsevier.com/retrieve/pii/S1352231005000087.
[57] M. Iqbal, Solar Radiation Measuring Instruments, Academic Press, 1983, https://doi.org/10.1016/B978-0-12-373750-2.50017-3. ISBN 978-0-12-373750-2, doi:\let\@tempa\bibinfo@X@, http://linkinghub.elsevier.com/retrieve/pii/B9780123737502500173.
[58] E. Gramsch, G. Le Nir, M. Araya, M.A. Rubio, F. Moreno, P. Oyola, Influence of large changes in public transportation (Transantiago) on the black carbon pollution near streets, Atmos. Environ. 65 (2013) 153–163, https://doi.org/10.1016/j.atmosenv.2012.10.006. ISSN 13522310, doi:\let\@tempa\bibinfo@X@, http://linkinghub.elsevier.com/retrieve/pii/S1352231012009600.
[59] M.A. Peña, Relationships between remotely sensed surface parameters associated with the urban heat sink formation in Santiago, Chile, Int. J. Remote Sens. 29 (15) (2008) 4385–4404, https://doi.org/10.1080/01431160801908137. ISSN 01431161, doi:\let\@tempa\bibinfo@X@, http://www.tandfonline.com/doi/abs/10.1080/01431160801908137.
[60] O.E. García, J.P. Díaz, F.J. Expósito, A.M. Díaz, O. Dubovik, Y. Derimian, P. Dubuisson, J.C. Roger, Shortwave radiative forcing and efficiency of key aerosol types using AERONET data, Atmos. Chem. Phys. 12 (11) (2012) 5129–5145, https://doi.org/10.5194/acp-12-5129-2012. ISSN 16807316, doi:\let\@tempa\bibinfo@X@, www.atmos-chem-phys.net/12/5129/2012/.
[61] M.A. Yamasoe, N.M. do Rosario, K.M. Barros, Downward solar global irradiance at the surface in Sñao Paulo city-The climatological effects of aerosol and clouds, J. Geophys. Res. 122 (1) (2017) 391–404, https://doi.org/10.1002/2016JD025585. ISSN 21562202, doi:\let\@tempa\bibinfo@X@.
[62] A.R. Esteve, V. Estelles, M.P. Utrillas, J.A. Martínez-Lozano, Analysis of the aerosol radiative forcing over a Mediterranean urban coastal site, Atmos. Res. 137 (2014) 195–204, https://doi.org/10.1016/j.atmosres.2013.10.009. ISSN 01698095, doi:\let\@tempa\bibinfo@X@, http://linkinghub.elsevier.com/retrieve/pii/S0169809513002822.
[63] S. Bibi, K. Alam, F. Chishtie, H. Bibi, S. Rahman, Observations of black carbon aerosols characteristics over an urban environment: radiative forcing and related implications, Sci. Total Environ. 603–604 (2017) 319–329, https://doi.org/10.1016/j.scitotenv.2017.06.082. ISSN 18791026, doi:\let\@tempa\bibinfo@X@.
[64] M. D. Chou, P. H. Lin, P. L. Ma, H. J. Lin, Effects of aerosols on the surface solar radiation in a tropical urban area, J. Geophys. Res. Atmosphere 111(15), ISSN 01480227, doi:\let\@tempa\ bibinfo@X@doi10.1029/2005JD006910.
[65] E.F. Fernandez, A. Soria-Moya, F. Almonacid, J. Aguilera, Comparative assessment of the spectral impact on the energy yield of high concentrator and conventional photovoltaic technology, Sol. Energy Mater. Sol. Cells 147 (2016) 185–197, https://doi.org/10.1016/j.solmat.2015.12.003. ISSN 09270248, doi:\let\ @tempa\bibinfo@X@, https://linkinghub.elsevier.com/retrieve/pii/S0927024815006510.
[66] G. Litjens, Investigation of spectral effects on photovoltaic technologies by modelling the solar spectral distribution, Ph.D. thesis, https://dspace.library.uu.nl/handle/1874/280693, 2013.
[67] K. Nomura, K. Imai, Y. Ota, T. Minemoto, K. Nishioka, Effect of aerosols on performance of concentrator photovoltaics, Jpn. J. Appl. Phys. 54 (8) (2015), https://doi.org/10.7567/JJAP.54.08KE07, 08KE07, ISSN13474065, doi:\let\@tempa\bibinfo@X@, http://stacks.iop.org/1347-4065/54/i=8S1/a=08KE07?key= crossref.746dc8fd5ee0dceacc1d0712fd00c668.
[68] M. Theristis, E.F. Fernandez, C. Stark, T.S. O'Donovan, A theoretical analysis of the impact of atmospheric parameters on the spectral, electrical and thermal performance of a concentrating III-V triple-junction solar cell, Energy Convers. Manag. 117 (2016) 218–227, https://doi.org/10.1016/j.enconman.2016.03.036. ISSN 01968904, doi:\let\@tempa\bibinfo@X@, http://linkinghub.elsevier.com/retrieve/pii/S0196890416301650.
[69] N.L.A. Chan, H.E. Brindley, N.J. Ekins-Daukes, Impact of individual atmospheric parameters on CPV system power, energy yield and cost of energy, Prog. Photovolt. Res. Appl. 22 (10) (2014) 1080–1095, https://doi.org/10.1002/pip.2376. ISSN 1099159X, doi:\let\@tempa\bibinfo@X@.
[70] F. Toledo, C. Garrido, M. Díaz, R. Rondanelli, S. Jorquera, P. Valdivieso, AOT retrieval procedure for distributed measurements with low-cost sun photometers, J. Geophys. Res.: Atmosphere ISSN 21698996, doi:\let\@tempa\bibinfo@X@doi10.1002/2017JD027309, URL https://doi.wiley.com/10.1002/2017JD027309.